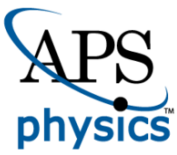

Electroconvection in a Viscoelastic Electrolyte

Gaojin Li, Lynden A. Archer, and Donald L. Koch

Phys. Rev. Lett. **122**, 124501 — Published 27 March 2019

DOI: 10.1103/PhysRevLett.122.124501

Electroconvection in a Viscoelastic Electrolyte

Gaojin Li, Lynden A. Archer and Donald L. Koch*
Smith School of Chemical and Biomolecular Engineering, Cornell University, Ithaca, NY 14853, USA
(Dated: March 6, 2019)

Direct numerical simulations of a liquid electrolyte with polymer additives demonstrate that viscoelasticity promotes an earlier transition from steady to unsteady electroconvective flow. Viscoelasticity also decreases the overlimiting current resulting from convection by up to 40%. Both of these effects would reduce the time-averaged spatial variability of ion flux suggesting that polymeric fluids may inhibit dendrite growth. Polymer relaxation near a surface destabilizes the flow structures and decreases the time duration of high current fluxes. This mechanism of polymer-induced flux reduction is general to wall bounded flows with transfer of mass, heat or momentum.

Electroconvective flow (ECF) in a liquid electrolyte near an ion-selective interface is important in electrodialysis [1], desalination [2], electrodeposition, and electrical energy storage in batteries [3, 4]. This phenomenon, in which the extended space charge layer (ESCL) plays a central role is distinct from ECF driven by interfacial charges or conductivity gradients in weakly conducting fluids [5–7] or the local tangential variation of potential and ion concentration due to the electrophoretic deposition of colloids [8]. Above a critical voltage, the electrohydrodynamic instability generates an electro-osmotic slip velocity at the edge of the ESCL [9], creating convective flows in the electrolyte [10–12] which cause an overlimiting current and a non-uniform ion flux. In both advanced batteries with metal anodes and fast charging Li-ion battery technology, non-uniform deposition of cations and its coupling with the ECF [4, 13] can lead to fast dendrite growth on the electrode and pose many issues [14].

Different strategies have been proposed to reduce the overlimiting current and suppress dendrite growth including the use of a gel membrane [15] or a solid electrolyte of cross-linked polymers [16]. Compared to solid electrolytes, liquid electrolytes have lower cost, higher ionic conductivity and better scalability, which makes them more desirable. A recent experiment showed that adding high molecular weight polymers to a liquid electrolyte can also delay the onset of the overlimiting current, suppress electroconvection, and stabilize uniform deposition [17]. It was seen that polymers have a small effect on the ionic conductivity while substantially increasing the solution viscosity, which based on a stability analysis [18, 19] would increase the critical voltage for ECF. Motivated by the favorable effects of solid elasticity in porous or gel-like media [15, 16], we postulate that fluid elasticity may also have advantages. Polymer viscoelasticity will be especially high in the ESCL where the fluid velocity $U \sim 10\mu\mathrm{m}/s$ and thickness $\varepsilon \sim 1\mu$m leads to Weissenberg number $\mathrm{Wi} = U\lambda/\varepsilon \sim \mathrm{O}(10 - 10^2)$ for polymer relaxation times $\lambda \sim 1 - 10$s [17]. In other settings, such high values of Wi can lead to turbulent flow even at a negligible Reynolds number [20], modify the heat transport in a Rayleigh-Bénard flow [21, 22], and cause significant drag reduction in a turbulent channel flow [23].

In this Letter, we study the effects of polymer elasticity on the ECF and show that polymer stress produced by interacting electroconvective vortices reduces the overlimiting current even though it may increase the fluid velocity. The fluid elasticity destabilizes the steady convective flow, reduces the time duration of high current fluxes and leads to a more uniform ion flux at the interface. On this basis, we contend that viscoelastic electrolytes with high extensional viscosity and large relaxation time are promising candidates for achieving uniform, dendrite-free electrodeposition in metal plating processes and in batteries. The study also provides insights into the general mechanism of polymer-induced flux reduction observed in many other contexts including Rayleigh-Bénard [21] and turbulent channel flow [23].

We perform two-dimensional simulations of a binary univalent electrolyte between an ion-selective surface and a stationary reservoir to model the LiTFSI electrolyte used in the experiments [17]. Previous studies suggest that 2D simulations capture the key features of ECF [24, 25] including the magnitude of the overlimiting current [25] and the primary mechanism of the ECF is not affected by additional supportive ions in the electrolyte [8]. To isolate the effects of polymer elasticity, the polymer is simulated using the FENE-CR model which allows finite extensibility of the polymer with no shear thinning [26]. The electrolyte is initially in a quiescent state with a uniform bulk concentration c_b. The governing equations for the incompressible fluid, electric potential, ion transport, and polymer deformation are

$$\mathrm{Re}\frac{\partial \boldsymbol{u}}{\partial t} = -\nabla p + \boldsymbol{f}_e + \nabla\cdot(\boldsymbol{\tau}^v + \boldsymbol{\tau}^p), \qquad \nabla\cdot\boldsymbol{u} = 0, \tag{1a}$$

$$-2\delta^2\nabla^2\phi = \rho, \tag{1b}$$

$$\mathrm{Pe}\frac{\partial c^{\pm}}{\partial t} + \nabla\cdot\boldsymbol{i}^{\pm} = 0, \tag{1c}$$

$$\frac{\partial \mathbf{A}}{\partial t} + \boldsymbol{u}\cdot\nabla\mathbf{A} - \nabla\boldsymbol{u}^{\mathrm{T}}\cdot\mathbf{A} - \mathbf{A}\cdot\nabla\boldsymbol{u} = \frac{f}{\mathrm{De}}(\mathbf{I} - \mathbf{A}). \tag{1d}$$

where $\boldsymbol{u}$ is the fluid velocity, p the pressure, $\boldsymbol{f}_e = -\rho\nabla\phi/2\delta^2$ the electrostatic force. ϕ the electric potential, $\rho = c^+ - c^-$ the free charge density, and $c^\pm$ the concentrations of cation and anion. $\delta = \sqrt{\varepsilon kT/(2e^2c_b)}/H$ is the dimensionless thickness of the electrical double layer (EDL), H, ε, k, T and e are the gap distance, dielectric permittivity, Boltzmann constant, temperature and elementary charge, respectively. $\boldsymbol{i}^\pm = \mathrm{Pe}c^\pm\boldsymbol{u} - \nabla c^\pm \mp c^\pm\nabla\phi$ are the fluxes of cation and anion, and the total electric current is $\boldsymbol{i} = \boldsymbol{i}^+ - \boldsymbol{i}^-$. $\boldsymbol{\tau}^v = 2(1-\beta)\mathbf{S}$ is the viscous stress, $\mathbf{S} = (\nabla\boldsymbol{u}^{\mathrm{T}} + \nabla\boldsymbol{u})/2$ is the strain-rate-tensor and $\beta = \mu^p/\mu$ is the ratio of the polymer viscosity μ^p to the total viscosity μ. The polymer stress for the FENE-CR model is $\boldsymbol{\tau}^p = \beta f(\mathbf{A}-\mathbf{I})/\mathrm{De}$, $\mathbf{A}$ is the conformation tensor and $f = 1/(1-\mathrm{tr}(\mathbf{A})/L^2)$ constrains the maximum extension L of the polymer.

In the equations, lengths are non-dimensionalized by H, velocity by $U_0 = \varepsilon(kT)^2/(e^2\mu H)$, time by H/U_0, ion concentration by c_b, and potential by kT/e. The Reynolds number $\mathrm{Re} = \rho_0 U_0 H/\mu = 5\times10^{-4}$ so we can neglect the convection term in the momentum equation, ρ_0 is the fluid density. The Peclet number $\mathrm{Pe} = U_0H/D$, which determines the onset of the overlimiting current [18, 27], is fixed to 0.5 unless otherwise mentioned, D is the diffusivity for both cation and anion. The Deborah number $\mathrm{De} = \lambda U_0/H$, which is the ratio of the polymer relaxation time λ and the flow time H/U_0, is the key parameter in this study and ranges from 0 to 5×10^{-2}. Other non-dimensional parameters include domain width $W = 6$, applied potential $V = 20-80$, $\beta = 0.5$, $L = 10^3$ and $\delta = 5\times10^{-4} - 10^{-2}$. The boundary conditions are $\boldsymbol{u} = 0, c^+ = 2, i_y^- = 0, \phi = 0$ at the ion-selective interface $y = 0$ and $\boldsymbol{u} = 0, c^+ = c^- = 1, \phi = V, \mathbf{A} = \mathbf{I}$ at $y = 1$. Equ. (1) are solved in a 2D domain using a hybrid spectral / finite volume method following previous studies of Newtonian electroconvection [12, 28, 29], the polymer conformation tensor is solved using the elastic and viscous stress splitting method [30] and a technique using a matrix-logarithm of the conformation tensor [31].

Polymer elasticity does not affect the onset of ECF [19], but it facilitates the transition from steady to unsteady convection and promotes a more uniform ion flux. At a small voltage $V = 20$ (Fig. 1*a*), steady vortex pairs emerge in a Newtonian fluid and form local hot spots of high cation flux by convecting the high salt concentration toward the electrode. The flow becomes unsteady in a viscoelastic fluid (Fig. 1*b*) and the time-averaged hot spots are flattened (see Supplemental Material Fig. S1). In steady ECF, each vortex is driven by an electroosmotic slip velocity u_s [27] in a manner similar to a lid-driven cavity flow, for which the critical Deborah number for the onset of unsteady flow is determined by the vortex turnover time $1/u_s$ following an empirical relation $\mathrm{De}_c = 1/[(\Lambda a + b)u_s]$, where $a = 0.14$ and $b = 2.8$ are two fitting constants characterizing the curvature of the streamlines given in [33], Λ is the ratio of the height

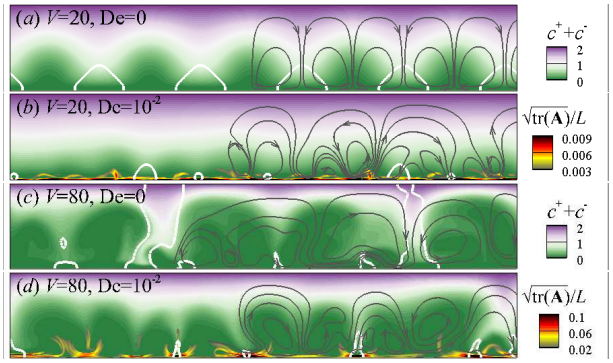

FIG. 1. Electroconvection for (*a*) $V = 20, \mathrm{De} = 0$, (*b*) $V = 20, \mathrm{De} = 10^{-2}$, (*c*) $V = 80, \mathrm{De} = 0$, (*d*) $V = 80, \mathrm{De} = 10^{-2}$; $\delta = 10^{-3}$. Contour plots show salt concentration c and polymer extension $\sqrt{\mathrm{tr}(\mathbf{A})}/L$, gray lines are streamlines, and the white contour lines indicate high flux regions with $i_y^+ = -3$ in (*a*, *b*) and -10 in (*c*, *d*), respectively. Movies are available in the Supplemental Material [32].

to the width of the vortex. We chose u_s to be the peak value of the standard deviation of the horizontal velocity $\sigma_u(y) = \langle\overline{u^2}\rangle^{1/2}$ (Inset of Fig. 2*b*) and the angle brackets and overbar are averages over x-direction and time, respectively. Simulations find u_s increases with decreasing δ, and it follows a linear relation with voltage $u_s \sim 6.1V - 93$ for $\delta = 10^{-3}$. Steady convection is observed in a Newtonian fluid with $V = 20, \delta = 10^{-3}$ and $V = 40, \delta = 10^{-2}$, for which $\Lambda = 1.67$ and 1.25 and $u_s \sim 30$ and 50, respectively. Based on these values, we derive $\mathrm{De}_c \sim 0.01$ and 0.007 which are consistent with the De at which the ECF becomes time periodic as indicated by the non-zero standard deviation of the current shown in the inset of Fig. 2*a*.

At a higher voltage such as $V = 80$, the convection is chaotic even in a Newtonian fluid (Fig. 1*c*) and the primary effect of the polymer is to suppress high ion flux regions. The strong, unsteady convection in a Newtonian fluid mixes the ions throughout the bulk region and results in bursts of high current spanning the gap. In the viscoelastic flow, streaks of extended polymers emerge in the regions of downward flow near the bottom surface and reduce the size of the low salt concentration blobs and the peak ion fluxes. The polymer only reaches about 10% of its maximum extension, suggesting that unsteadiness rather than finite extensibility is limiting the polymer stress (Fig. 1*d*). This thin layer of strong polymer extension could be the reason for the second interfacial resistance observed in the experiments [17].

The effects of polymer stress on the ECF can be quantified using the Weissenberg number $\mathrm{Wi} = \mathrm{De}u_s/\epsilon$, which characterizes the extension of the polymer due to the high shear rate u_s/ϵ in the ESCL. Previous analysis for the Newtonian electrolyte showed that the ESCL thickness $\epsilon \sim (V\delta)^{2/3}$ [27] and we estimate ϵ as the y location of the peak value of $\sigma_u(y)$ (Inset of Fig. 2*b*). Fig. 2

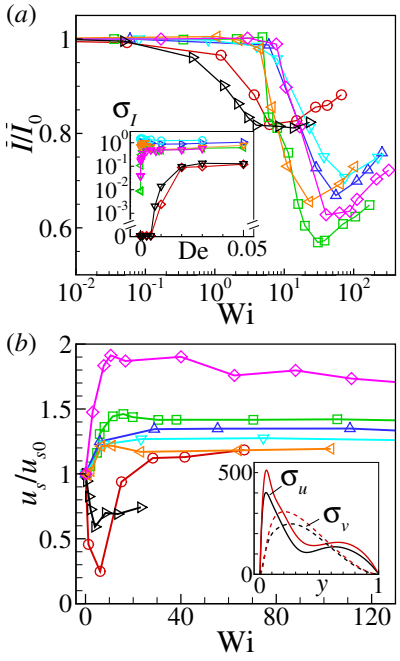

FIG. 2. (a) The normalized average current density $\bar{I}/\bar{I}_0$ and (b) slip velocity u_s/u_{s0} vs Wi. ◯, □, △, ▽ represent $V = 20, 40, 60, 80$ with $\delta = 10^{-3}$, ▷, ◁ and ◇ represent $V = 40$ with $\delta = 10^{-2}, 2\times10^{-3}$ and 2×10^{-4}, respectively. Inset in (a): Standard deviation of current σ_I vs De. Inset in (b): Standard deviation of fluid velocity σ_u and σ_v vs y for $V = 80$, black and red lines represent De $= 0$ and 10^{-2}, respectively.

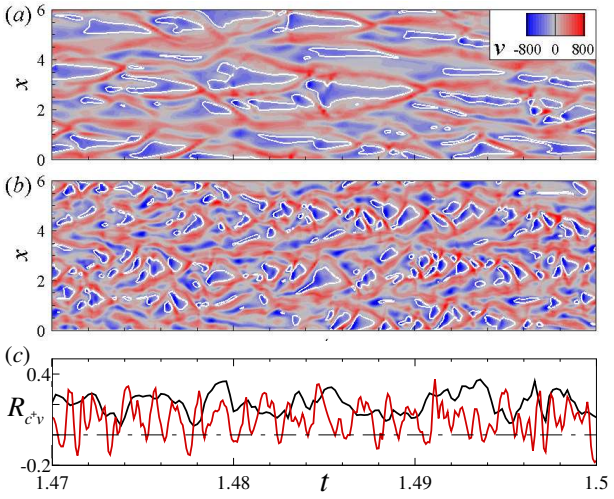

FIG. 3. Spatiotemporal evolution of the flow field at $y = 0.2$ in (a) Newtonian and (b) viscoelastic fluid with Wi $= 74.6$ at $V = 80$ and $\delta = 10^{-3}$. The color shows the normal velocity component v and white contourlines represent the regions of high cation flux with $i_y^+ = -15$. (c) Time history of cross-correlation of c^+ and v at $y = 0.2$ for Newtonian (black) and viscoelastic fluids (red).

shows the normalized average current $\bar{I}/\bar{I}_0$ and slip velocity u_s/u_{s0} vs Wi, where $I = -\langle i_y|_{y=0}\rangle$ is the space-average current density, $\bar{I}_0$ and u_{s0} are the current and slip velocity at De $= 0$. The current decreases beyond a critical Weissenberg number, Wi_c, reaches a maximum reduction of up to 40% and then slowly increases with increasing Wi. Two distinct values Wi_c are observed, $\mathrm{Wi}_c \sim$ O(0.1) for the two cases of steady Newtonian vortices, and $\mathrm{Wi}_c \sim$ O(10) for the cases with unsteady Newtonian flows. The current reduction occurs within the range of Weissenberg numbers explored in the experiments [17].

The fact that Wi_c depends on the state of the Newtonian ECF suggests there exist two different mechanisms of current reduction. This is also evident from the behavior of the slip velocity u_s. In Fig. 2b, u_s initially decreases with increasing Wi for flows with steady convection at Wi=0, while it increases for all other cases. The concurrence of current and convection reductions indicates an increment of the viscosity of the electrolyte. In a stationary flow, the regions where two vortices abut near the bottom surface are locally extensional. The extensional viscosity of the polymer increases with Wi following $\mu_e \sim 4\mu(1+4\beta\mathrm{Wi}^2)$ for Wi < 0.5. After Wi > 0.5, the polymers are dramatically stretched, limited only by the finite extensibility, and the viscosity approaches the asymptote $\mu_e \sim 4\mu(1+0.5\beta L^2)$ [26]. The local high viscosity resists electroconvection and reduces the current.

At higher V where the Newtonian flow is unsteady, the polymer generates smaller and shorter lived vortices (see Fig. S2) and increases u_s. The increment of u_s is large in a flow with a small ESCL, indicating that this effect may be more dramatic in a real battery. The inset compares the standard deviation of the fluid velocity for Wi $= 0$ and 74.6 (De $= 10^{-2}$) at $V = 80$. Viscoelasticity also increases the vertical velocity, which directly transports ions to the surface. All previous studies in Newtonian fluids indicated that the overlimiting current increased when the electroconvection became stronger [12, 34]. Our results show this is not generally true in a viscoelastic fluid.

To understand how the polymer reduces the current density in an unsteady flow, we compare the spatiotemporal evolution of Newtonian (Fig. 3a) and maximum-reduced-current (Fig 3b) flow fields for $V = 80$ at $y = 0.2$. This location is outside the ESCL and has the largest vertical velocity v as shown in Fig. 2b. The irregular structures formed by the fluid velocity demonstrate the chaotic nature of the convective flow, in which the vortices constantly reposition, merge and break down. The high cation flux only occurs in regions of strong downward flow and the peak current can grow to about 10 times the average current density. In a Newtonian fluid, the time duration of a high flux spot is typically $\Delta t \sim 3\times10^{-3}$, which is near the eddy turnover time of the dominant vortices $\sim 1/u_s = 2.5\times10^{-3}$. In a polymer solution, the polymers form streaks of large poly-

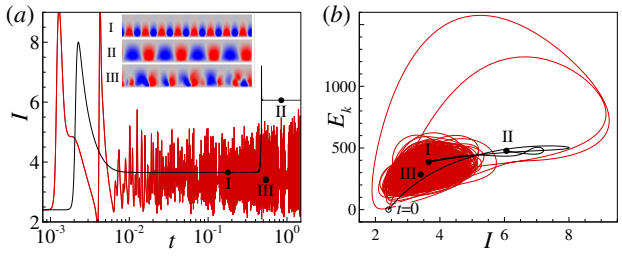

FIG. 4. (a) Time history of the average current I and (b) phase diagram of I vs fluid kinetic energy E_k for De = 0 (black) and 10^{-3} (red); $V = 80, \delta = 10^{-3}$ and Pe = 0.05. Points I and II represent the two states in the Newtonian flow, and point III marks the average values of I and E_k in the polymer flow. The insets in (a) show the normal velocity.

mer extension in a downward flow region. These streaks cannot be stably sustained and their relaxation generates a reverse flow that quickly terminates the high ion flux. The duration $\Delta t \sim 10^{-3}$ and prevalence of the high ion flux in a polymer flow are both reduced by this mechanism. In addition to attenuating the highest flux regions, the polymer induces flow unsteadiness and reduces concentration-velocity correlations throughout the fluid. The average cation flux due to convection, which can be written as $I_c^+ = \langle c^{+2}\rangle^{1/2}\langle v^2\rangle^{1/2} R_{c^+v}$, is sensitive to the cross-correlation R_{c^+v} of the cation concentration and vertical velocity. The polymer destabilizes downwelling flows that would have produced correlations between negative v and high c^+ near the bottom surface thereby reducing the average current density (Fig. 3c). Similar results are found at a lower voltage $V = 20$ (see Fig. S3).

From the viewpoint of dynamical system, the ECF consists of states with large size vortices and high current and states with small vortices and low current, and the polymer decreases the occurrence rate of the states with large vortices. In an ECF of lower Pe = 0.05 and slower time evolution, the Newtonian fluid eventually transits from state (I) of small vortices to a new state (II) of larger vortices whose size is near the gap distance, and the current increases from $\bar{I} = 3.7$ to 6.1. In a polymer solution, the polymer stretching and relaxation repeatedly destabilizes the larger vortices with $\bar{I} = 3.4$, and the system is attracted to the low current state (Fig. 4).

The polymer-induced flux reduction in an ECF is comparable to that in polymeric Rayleigh-Bérnard (RBF) and turbulent channel flow (TCF). In all three flows, instability-enhanced flux (of ion, heat and momentum, respectively) naturally occurs when the destabilizing force (electrostatic, buoyancy and inertia) overcomes the stabilizing viscous force. Furthermore, polymers reduce the flux in all three flows at high enough Wi [21, 35]. Although polymers enhance the heat transfer in RBF without boundaries [22], the heat flux is reduced by polymers in the presence of boundaries [21] and, as in ECF, the reduction passes through a maximum at a certain Wi [36]. In both ECF and TCF, the large shear rate near the wall generates streaks of strong polymer stretching parallel to the wall [37], the kinetic energy spectrum scales as $E_k \sim k_x^{-5}$ at high wavenumbers (see Fig. S4) [38, 39], and the polymer modulates the transition between active and hibernating states with high and low fluxes [35]. Our result shows that similar effects can be achieved at negligible Reynolds number and without a mean flow. The polymer stress destabilization of the flow structures producing high fluxes is the key to reducing transport near a surface.

Using direct numerical simulations, we have shown that viscoelastic polymer additives to a liquid electrolyte can improve the uniformity of ion flux at an ion-selective interface. At a relatively low voltage, polymers destabilize the steady convective flow, resulting in chaotic convection that leads to a more uniform ion flux to the surface. At higher voltages, the polymers reduce the overlimiting current by up to 40% even while increasing the fluid velocity. Our results indicate that the strong resistance of polymers to extensional motion alters the flow structures so as to decrease the time duration of high current fluxes. The analogies between the viscoelastic effect observed in ECF and other flows may contribute to an understanding of the general mechanism by which polymers reduce transport in wall-bounded flows.

The authors thank Ali Mani for his invaluable help during the development of the numerical code. This research is supported by Department of Energy Basic Energy Science Grant DE-SC0016082.

* dlk15@cornell.edu

[1] I. Rubinstein, B. Zaltzman, and O. Kedem, J. Membr. Sci. **125**, 17 (1997).
[2] S. J. Kim, S. H. Ko, K. H. Kang, and J. Han, Nat. Nanotechnol. **5**, 297 (2010).
[3] V. Fleury, J. N. Chazalviel, and M. Rosso, Phys. Rev. E **48**, 1279 (1993).
[4] J. M. Huth, H. L. Swinney, W. D. McCormick, A. Kuhn, and F. Argoul, Phys. Rev. E **51**, 3444 (1995).
[5] J. R. Melcher and G. I. Taylor, Annu. Rev. Fluid Mech. **1**, 111 (1969).
[6] D. A. Saville, Annu. Rev. Fluid Mech. **29**, 27 (1997).
[7] H. Lin, B. D. Storey, M. H. Oddy, C.-H. Chen, and J. G. Santiago, Phys. Fluids **16**, 1922 (2004).
[8] M. Trau, D. A. Saville, and I. A. Aksay, Langmuir **13**, 6375 (1997).
[9] I. Rubinstein and B. Zaltzman, Math. Models Meth. Appl. Sci. **11**, 263 (2001).
[10] S. M. Rubinstein, G. Manukyan, A. Staicu, I. Rubinstein, B. Zaltzman, R. G. H. Lammertink, F. Mugele, and M. Wessling, Phys. Rev. Lett. **101**, 236101 (2008).
[11] E. A. Demekhin, N. V. Nikitin, and V. S. Shelistov, Phys. Fluids **25**, 122001 (2013).
[12] C. L. Druzgalski, M. B. Andersen, and A. Mani, Phys.

Fluids **25**, 110804 (2013).
[13] L. Sundström and F. H. Bark, Electrochim. Acta **40**, 599 (1995).
[14] M. D. Tikekar, S. Choudhury, Z. Tu, and L. A. Archer, Nat. Energy **1**, 16114 (2016).
[15] F. Maletzki, H. W. Rösler, and E. Staude, J. Membr. Sci. **71**, 105 (1992).
[16] R. Khurana, J. L. Schaefer, L. A. Archer, and G. W. Coates, J. Am. Chem. Soc. **136**, 7395 (2014).
[17] S. Wei, Z. Cheng, P. Nath, M. D. Tikekar, G. Li, and L. A. Archer, Sci. Adv. **4**, eaao6243 (2018).
[18] I. Rubinstein and B. Zaltzman, Phys. Rev. E **62**, 2238 (2000).
[19] M. D. Tikekar, G. Li, L. A. Archer, and D. L. Koch, J. Electrochem. Soc. **165**, A3697 (2018).
[20] A. Groisman and V. Steinberg, Nature **405**, 53 (2000).
[21] G. Ahlers and A. Nikolaenko, Phys. Rev. Lett. **104**, 034503 (2010).
[22] R. Benzi, E. S. C. Ching, and E. De Angelis, Phys. Rev. Lett. **104**, 024502 (2010).
[23] C. M. White and M. G. Mungal, Annu. Rev. Fluid Mech. **40**, 235 (2008).
[24] C. Druzgalski and A. Mani, Phys. Rev. Fluids **1**, 073601 (2016).
[25] E. A. Demekhin, N. V. Nikitin, and V. S. Shelistov, Phys. Rev. E **90**, 013031 (2014).
[26] M. D. Chilcott and J. M. Rallison, J. Non-Newton. Fluid Mech. **29**, 381 (1988).
[27] I. Rubinstein, B. Zaltzman, and I. Lerman, Phys. Rev. E **72**, 011505 (2005).
[28] E. Karatay, C. L. Druzgalski, and A. Mani, J. Colloid Interface Sci. **446**, 67 (2015).
[29] C. Druzgalski, *Direct Numerical Simulation of Electroconvective Chaos Near an Ion-selective Membrane*, Ph.D. thesis, Stanford University (2016).
[30] R. Guénette and M. Fortin, J. Non-Newton. Fluid Mech. **60**, 27 (1995).
[31] R. Fattal and R. Kupferman, J. Non-Newton. Fluid Mech. **123**, 281 (2004).
[32] Supplemental Material at http://link.aps.org/..
[33] P. Pakdel and G. H. McKinley, Phys. Rev. Lett. **77**, 2459 (1996).
[34] M. B. Andersen, K. M. Wang, J. Schiffbauer, and A. Mani, Electrophoresis **38**, 702 (2017).
[35] M. D. Graham, Phys. Fluids **26**, 625 (2014).
[36] J. P. Cheng, H. N. Zhang, W. H. Cai, S. N. Li, and F. C. Li, Phys. Rev. E **96**, 013111 (2017).
[37] T. Min, J. Y. Yoo, H. Choi, and D. D. Joseph, J. Fluid Mech. **486**, 213 (2003).
[38] L. Thais, G. Mompean, and T. B. Gatski, J. Non-Newton. Fluid Mech. **200**, 165 (2013).
[39] Y. Dubief, V. E. Terrapon, and J. Soria, Phys. Fluids **25**, 110817 (2013).